Towards numerical simulations of trailing-edge aeroacoustics

By Meng Wang

1. Motivation and objectives

The aeroacoustics of flow-hydrofoil interactions exhibits distinct characteristics depending on the physical length scales involved. In the small-foil (relative to acoustic wavelength) limit characteristic of the noise generated by large-scale vortex shedding at low flow Mach number, the noise calculation is facilitated by the use of the Lighthill analogy (Lighthill 1952) in conjunction with a free-space Green's function, in the sense of Curle's formulation (Curle 1955). A methodology for computing the vortex-shedding noise using the Curle formulation, including both surface-induced dipole sources and volume quadrupole sources, has been developed. The completed work, emphasizing the importance of an adequate outflow boundary treatment for accurate volume source calculation, can be found in Wang (1995) and Wang, Lele & Moin (1996).

A more fascinating aspect of the hydrofoil noise is the aeroacoustic scattering by the trailing edge, or the interaction of turbulent-boundary-layer eddies with the trailing edge. This occurs at the large-body limit, i.e., when the hydrofoil chord is comparable with or exceeds the dominant acoustic wavelength, and is the source of intense, broad-band noise (Brooks & Hodgson 1981; Blake & Gershfeld 1988). Our ongoing research is focused on this flow regime. The presence of a sharp trailing edge enhances the acoustic-energy radiation to the far-field by altering the source characteristics; for instance, turbulent eddies, known as quadrupole sources in free space, behave in a non-multipole (sometimes termed "3/2-pole") fashion in the vicinity of a semi-infinite flat-plate edge (Ffowcs Williams & Hall 1970). Crighton & Leppington (1971) show that the non-multipole character of the radiated field is caused by the fact that the scattering surface is noncompact relative to the acoustic wavelength. To account for the surface reflection effect, a hard-wall Green's function, whose normal derivative vanishes on the surface, must be employed in an integral solution to the Lighthill equation. Howe (1978) gives an extensive review of the theoretical developments in trailing-edge noise prediction methods.

In addition to the directly radiated aerodynamic noise, the fluctuating wall-pressure (pseudo-sound) field is of importance in practical applications since it tends to excite structural vibrations and low frequency noise (Blake 1986). The space-time characteristics of wall-pressure fluctuations are frequently required as a forcing-function input for various structural models. The rapid changes in surface pressure near the trailing edge provides an efficient mechanism for generating the detrimental lower-frequency content of the wall-pressure wavenumber spectrum. The problem is often further complicated by the presence of adverse pressure gradient, boundary-layer separation, and vortex shedding in the trailing-edge region.

Blake (1975) and Blake & Gershfeld (1988) conducted a series of aeroacoustic experiments with lifting hydrofoils which have asymmetrically beveled trailing edges. The asymmetric edge shape produced a separated flow on the low-pressure side, and an attached boundary layer on the high-pressure side. Measurements were made of the turbulent velocity fields near the trailing edge, fluctuating surface pressures, and radiated noise signals. Correlation and cross-spectral analyses were conducted between the velocity and pressure signals in an attempt to determine the physical mechanisms for generating unsteady surface pressure and radiated noise. Brooks & Hodgson (1981) measured the scattered surface pressure fields near the trailing edges and the radiated fields, of flows past a NACA 0012 airfoil at several angles of attack and with varying degrees of edge bluntness. The cross-spectral analysis of the measured noise data pointed to the trailing edge region as the dominant noise source. In the case of a sharp edge, excellent agreement with theoretical predictions in terms of the U_∞^5-dependence (U_∞ is the free-stream velocity) of sound intensity and the $\sin^2(\theta/2)$ (θ is defined in Fig. 5) directivity was obtained.

Well designed experiments are invaluable in validating theory and providing insight into the complex edge-noise phenomena. However, they are limited in terms of providing detailed, global information about the flow field, and frequently resort to *a priori* assumptions regarding acoustic source mechanisms in order to reduce the amount of data to be collected. There is a pressing need for developing numerical simulation capabilities and accurate numerical databases to facilitate the acoustic source analysis. As a preliminary attempt, Zawadzki *et al.* (1996) used the database of Na & Moin (1996) for a separated, flat-plate turbulent boundary layer to examine the acoustic forcing functions, arguing that the separated boundary layer has characteristics similar to those of the boundary layer incident to a hydrofoil trailing-edge on the suction side. There are, however, important aspects of the trailing edge flow, such as pressure scattering, that the flat-plate boundary layer does not include.

The objectives of the present work are twofold. First, we aim to develop a computational method for the prediction of trailing-edge noise and wall-pressure fluctuations. The general approach consists of a large eddy simulation (LES) of the turbulent near-field (the boundary layers and the near wake), in combination with a suitable formulation of aeroacoustic theory for the evaluation of the acoustic source functions and the radiated field. The second goal is to study the physical mechanisms for the generation of sound and pseudosound. Besides the edge scattering effect, we are also interested in the roles played by pressure gradients, boundary-layer separation, and the lifted shear-layer.

2. Accomplishments

2.1 LES of trailing-edge turbulence

The flow configuration corresponds to one of Blake's experiments (Blake 1975). As shown in Fig. 1, where the contour lines denote the mean streamwise velocity from a Reynolds Averaged Navier-Stokes (RANS) calculation (to be discussed later), a two-dimensional hydrofoil with a beveled, 25-degree trailing edge is placed in a

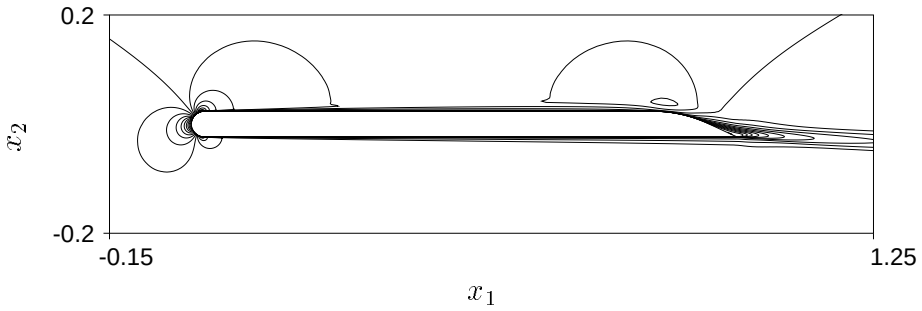

FIGURE 1. Flow past a hydrofoil with a 25-deg beveled trailing edge (the contour lines represent streamwise velocity obtained from a RANS calculation).

uniform stream at zero-degree angle of attack. The hydrofoil has a circular leading edge and a chord/thickness ratio of 21.125. The chord-based free-stream Reynolds number is 2.15×10^6. A more detailed definition of the geometry and experimental conditions can be found in Blake (1975).

Past experiences with airfoils at high Reynolds number (Jansen 1995, Kaltenbach & Choi 1995) indicate that a full-scale LES with the entire foil would be too costly and suffer from inadequate grid resolution. In particular, laminar separation near the nose and the ensuing transition to turbulence pose an extremely stringent resolution requirement. Since the major interest in the present study is the trailing-edge region, we opted for a simulation which includes only the aft section ($\sim 38\%$ chord length) of the foil and the near wake. The computational grid for a preliminary simulation is depicted in Fig. 2. For clarity, only one in every four grid lines is plotted, and the domain has been truncated in the vertical direction. The actual domain size, in terms of maximum thickness of the hydrofoil, is approximately $20 \times 82 \times 0.5$ in the streamwise (x_1), normal (x_2), and spanwise (x_3) directions, respectively. A total of $288 \times 160 \times 32$ effective computational cells are employed, with mesh refinements near the surface and the trailing edge.

The numerical method employed in the present study is described in Choi (1993) and Mittal (1996). Second-order central difference is used for spatial discretization on a staggered mesh in curvilinear coordinates in the x_1-x_2 plane, and Fourier collocation with dealiasing is used for discretization in the Cartesian x_3 direction. The time-advancement is of the fractional step type, in combination with the Crank-Nicolson method for viscous terms and third order Runge-Kutta scheme for convective terms. The continuity constraint is imposed through a pressure Poisson equation, which is solved at each Runge-Kutta sub-step using a multi-grid iterative procedure. The subgrid-scale stress is modeled using the dynamic SGS model (Germano *et al.* 1991) in combination with least-square contraction (Lilly 1992), spanwise averaging, and a clipping operation to limit the total viscosity to positive values.

The numerical code, originally written for the C-type mesh, has been modified to accommodate an inflow-outflow configuration with a splitting wedge, as shown in Fig. 2. The modified code has been validated under simpler laminar flow conditions,

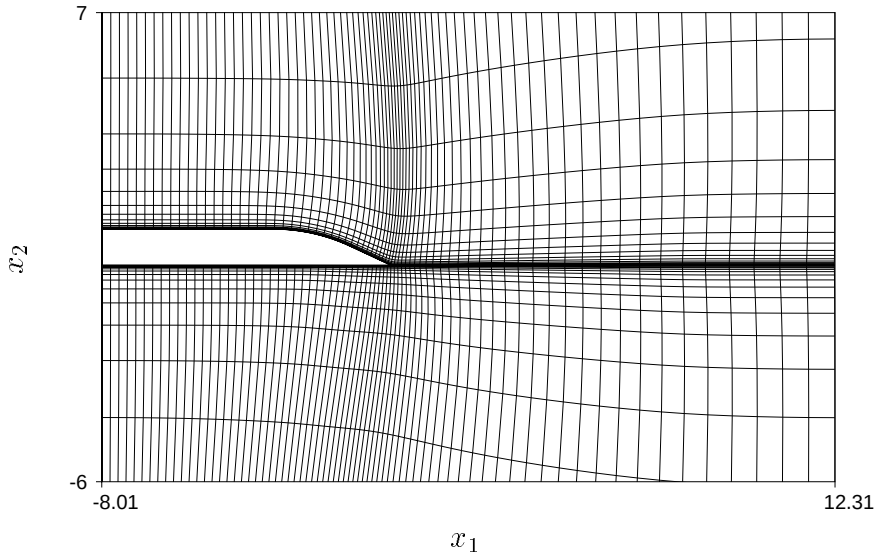

FIGURE 2. Computational grid for LES of trailing-edge flow. For clarity only one in every four grid lines is plotted.

including double (upper and lower surface) Blasius boundary layers, and linear amplifications of Tollmien-Schlichting waves.

The inflow boundary conditions pose a particular problem not encountered in a full-scale airfoil simulation. The mean velocity profiles at the upper and lower inlets differ from those of a flat-plate boundary layer due to flow acceleration. They are also affected by the presence of a mean circulation associated with a lifting surface. Unfortunately, the experimental measurements made by Blake (1975) were limited to the upper-side of the foil, and even there the available data are insufficient for boundary condition specification. As a result, we resorted to an auxiliary RANS calculation, using the k-ϵ-v^2 turbulence model (Durbin 1995) in a large domain enclosing the full hydrofoil. The resulting mean velocity data are used in setting up the velocity boundary conditions outside the boundary layers. As demonstrated in Fig. 3, the mean streamwise velocities at the inlets on two sides of the edge indeed deviate significantly from each other and from the free-stream velocity of unity. Serious errors will arise if the uniform free-stream velocity is imposed at both inlets.

The turbulent-boundary-layer inflow data are generated from two separate LES of flat-plate boundary layers with zero pressure gradient, on the basis that the pressure gradients from experiments and the RANS calculation are small at the given chord station. The inflow-generation procedure is described by Lund (1994). The inflow-generation LES employs an identical mesh resolution as the trailing-edge flow LES at the inlets and matches the local boundary layer properties, including the momentum thickness and Reynolds number, with those from the RANS simulation. A discrete time series of the three velocity components in an appropriate x_2-x_3 plane are saved to be later fed into the inflow boundaries of the main simulation.

A no-slip condition is applied to the surface of the foil. The top and bottom

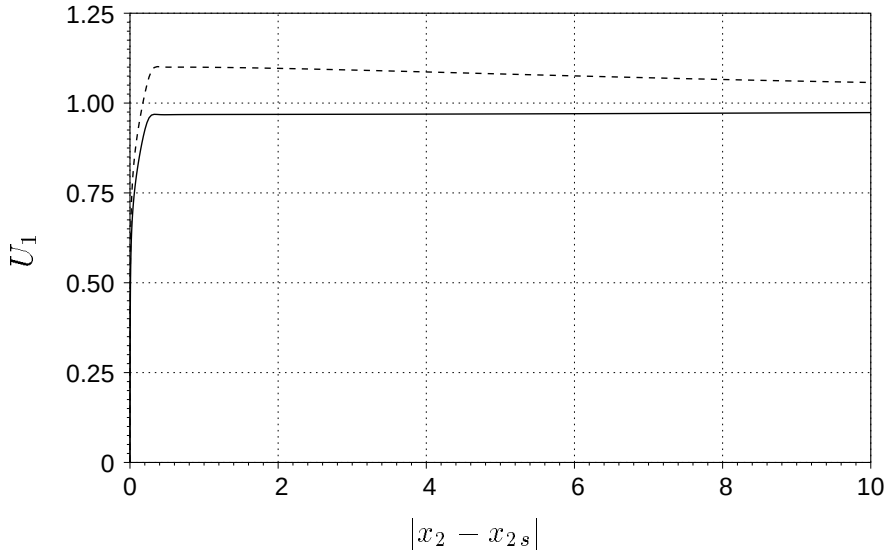

FIGURE 3. Mean streamwise velocities at LES inlets as a function of vertical distance from the foil surface, obtained from a RANS calculation. ——— lower inlet; - - - - upper inlet.

boundaries are placed far (41 foil thicknesses) away from the foil to minimize the impact of velocities imposed along these boundaries. We used the velocity distributions from the RANS calculation, which deviate from the free-stream velocity by less than two percent. At the downstream boundary the convective outflow condition (Pauley, Moin & Reynolds 1988) is applied to allow the vortical disturbances in the wake to leave the computational domain smoothly.

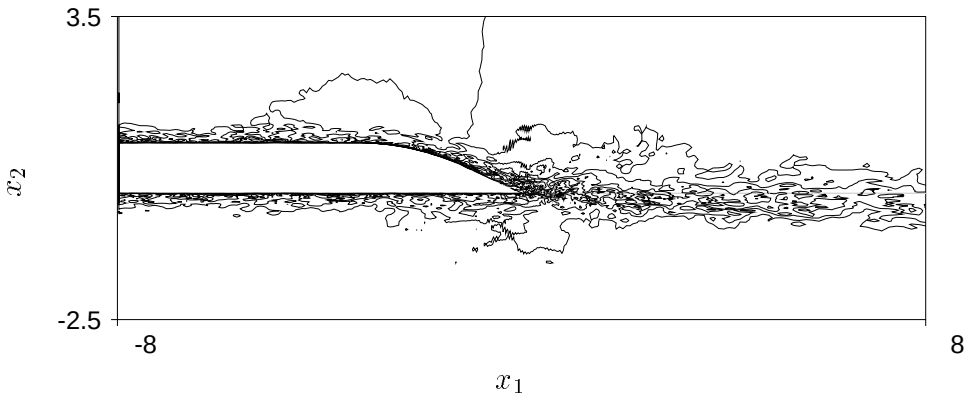

FIGURE 4. Contours of streamwise velocity u_1 in a constant x_3 plane, at $t = 29.2$. Contour levels from -0.1 to 1.3, increment 0.1.

The trailing-edge LES is presently in progress. As of this date the numerical integration has advanced approximately 1.5 flow-through times based on the free-stream velocity. It is too early to collect meaningful statistics. An instantaneous streamwise velocity field in mid-span is plotted in Fig. 4. One notices that there is

no visible flow separation on the suction side of the edge. This could be caused either by the initial transients still present at this stage of simulation or by insufficient spatial resolution in this preliminary run. The grid spacing in wall units is estimated to be $\Delta x^+_{2\,min} \approx 2$, $\Delta x^+_3 \approx 55$, and $\Delta x^+_1 \approx 220$ at inlets and 100 near the trailing edge. Thus, the resolution is quite poor compared with that of typical wall-bounded LES practices.

2.2 Acoustic formulation

A solution to the Lighthill equation in frequency domain can be expressed in terms of convolution integrals with an appropriate Green's function (Goldstein 1976),

$$\widehat{\rho}_a(\boldsymbol{x},\omega) = M^2 \int_V \widehat{T}_{ij}(\boldsymbol{y},\omega)\frac{\partial^2 G}{\partial y_i \partial y_j}(\boldsymbol{x},\boldsymbol{y},\omega)\,d^3\boldsymbol{y} + M^2 \int_S n_j \widehat{p}_{ij}(\boldsymbol{y},\omega)\frac{\partial G}{\partial y_i}(\boldsymbol{x},\boldsymbol{y},\omega)\,d^2\boldsymbol{y}, \tag{1}$$

where ρ_a denotes the density perturbation and the caret denotes temporal Fourier transform. $T_{ij} = \rho v_i v_j + \delta_{ij}\left(p - \rho/M^2\right) - \tau_{ij}$ is the Lighthill stress tensor defined in terms of the fluctuating velocity relative to the free-stream value ($v_i = u_i - \delta_{i1}$), the entropy (second term), and the viscous stress tensor τ_{ij}. $p_{ij} = p\delta_{ij} - \tau_{ij}$ is the compressive stress tensor, $\boldsymbol{x}$ and $\boldsymbol{y}$ are the coordinates of the observation point and the source point, respectively, and n_i denotes the directional cosine of the outward normal (into the fluid) to the rigid surface S over which the surface integration takes place. The volume integral is taken over the entire unsteady flow region V external to the body. G is the Green's function which satisfies the modified wave (Helmholtz) equation

$$\left(\frac{\partial^2}{\partial x_j \partial x_j} + k^2\right) G(\boldsymbol{x},\boldsymbol{y},\omega) = -\delta(\boldsymbol{x},\boldsymbol{y}) \tag{2}$$

and the appropriate boundary conditions. Equations (1) and (2) are written in a dimensionless form. The velocity, density, and pressure are nondimensionalized by the undisturbed free-stream values U'_∞, ρ'_∞, and $\rho'_\infty U'^2_\infty$, respectively. The spatial coordinates are normalized by the hydrofoil thickness h'. The frequency (ω) is normalized by U'_∞/h'. Re and M denote respectively the free-stream Reynolds number based on h' and the free-stream Mach number. δ_{ij} is the Kronecker delta, and the usual summation convention applies for repeated subscripts.

Except for the neglect of $O(M)$ bulk convection effect, (1) is exact and may serve as the starting point for studying the aeroacoustics of arbitrary flow-body interactions. For instance, the Curle integral (Curle 1955) is obtained if the free-space Green's function is used. A hard-wall Green's function, which satisfies $\partial G/\partial \boldsymbol{n} = 0$, is required for the calculation of acoustic scattering phenomenon. In general, an analytical expression for Green's function tailored to the complex, acoustically non-compact geometry such as the hydrofoil is nonexistent. Under certain asymptotic limits, however, one may use a known Green's function for a simpler geometry as an approximation.

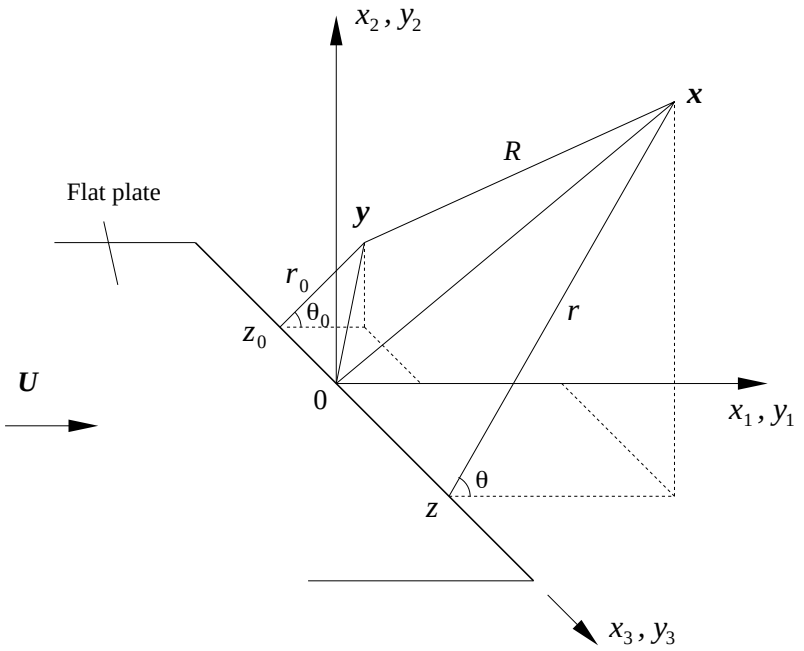

FIGURE 5. Coordinate system for calculating the radiated noise of flow past the trailing-edge of a semi-infinite flat plate.

In the limit that the hydrofoil thickness is much smaller than the acoustic wavelength ($h \ll \lambda_a$), the foil is reasonably approximated by a half-plane with zero thickness, for which the far-field Green's function is known (Ffowcs Williams & Hall 1970; Goldstein 1976):

$$G = \frac{e^{ikR}}{4\pi R}\left(\frac{1}{2} + \frac{e^{-i\frac{\pi}{4}}}{\sqrt{\pi}}\int_0^a e^{iu^2}du\right) + \frac{e^{ikR^*}}{4\pi R^*}\left(\frac{1}{2} + \frac{e^{-i\frac{\pi}{4}}}{\sqrt{\pi}}\int_0^{a^*} e^{iu^2}du\right). \tag{3}$$

In the above equation, the wavenumber $k = M\omega$, and the distances $R = |\boldsymbol{x} - \boldsymbol{y}|$ and $R^* = |\boldsymbol{x} - \boldsymbol{y}^*|$, where $\boldsymbol{y}^* = (y_1, -y_2, y_3)$. In the cylindrical coordinate system defined in Fig. 5,

$$R = \left[r^2 + r_0^2 - 2rr_0\cos(\theta - \theta_0) + (z - z_0)^2\right]^{\frac{1}{2}}, \tag{4}$$

$$R^* = \left[r^2 + r_0^2 - 2rr_0\cos(\theta + \theta_0) + (z - z_0)^2\right]^{\frac{1}{2}}, \tag{5}$$

$$a = (2kr_0\sin\phi)^{\frac{1}{2}}\cos\left(\frac{\theta - \theta_0}{2}\right), \tag{6}$$

$$a^* = -(2kr_0\sin\phi)^{\frac{1}{2}}\cos\left(\frac{\theta + \theta_0}{2}\right), \tag{7}$$

$$\sin\phi = \frac{r}{\left[r^2 + (z - z_0)^2\right]^{\frac{1}{2}}}. \tag{8}$$

For high Reynolds number flows, the viscous stress, entropy, and hence the surface integral are frequently neglected. Substituting (3)-(8) into (1) and retaining only the lowest order terms in M and R^{-1} lead to

$$\widehat{\rho}_a(\boldsymbol{x},\omega) \approx M^{\frac{5}{2}} \frac{e^{-i\frac{\pi}{4}}}{\pi^{\frac{1}{2}}} \int_V \frac{1}{4\pi R} \frac{(\omega \sin\phi)^{\frac{1}{2}}}{(2r_0)^{\frac{3}{2}}} \times \left\{ \left(\widehat{v_\theta^2 - v_r^2}\right) \left[e^{i\left(kR+a^2\right)} \cos\left(\frac{\theta-\theta_0}{2}\right) - e^{i\left(kR^*+a^{*2}\right)} \cos\left(\frac{\theta+\theta_0}{2}\right) \right] -2\widehat{v_r v_\theta} \left[e^{i\left(kR+a^2\right)} \sin\left(\frac{\theta-\theta_0}{2}\right) + e^{i\left(kR^*+a^{*2}\right)} \sin\left(\frac{\theta+\theta_0}{2}\right) \right] \right\} d^3\boldsymbol{y}. \quad (9)$$

The strongest far-field noise is generated by the fluctuating Reynolds stress components normal to the scattering edge in a cylindrical region of radius much smaller than the acoustic wavelength ($r_0 \ll \lambda_a$). Within this region, $e^{i\left(kR+a^2\right)} \approx e^{i\left(kR^*+a^{*2}\right)} \approx e^{ikR}$, and the simpler, more familiar form (Goldstein 1976) is recovered. Equation (9) is more suitable for numerical evaluations in that it allows the volume integration to be carried out to larger r_0 values. Since the integrand decays as $r_0^{-3/2}$, a large r_0 bound is beneficial in minimizing the spurious boundary noise caused by nonvanishing source terms at the computational boundary. As demonstrated by Wang *et al.* (1996), boundary errors can severely compromise the accuracy of an acoustic analogy based calculation.

The thin-foil limit ($h \ll \lambda_a$) discussed above covers the relatively low frequency (wavenumber) range of the radiated noise. Since $\lambda_a \sim l_e/M$, where l_e is the eddy size, the approximation is valid for $l_e/h \gg M$, a condition likely to be met by the range of eddies resolvable in the source-field LES, at typical Mach numbers in naval applications.

On the other hand, if $h \gg \lambda_a$, the trailing edge is approximately equivalent to a triangular wedge on the acoustic length scale. By using a conformal mapping technique, Crighton & Leppington (1971) showed that $\widehat{\rho}_a \sim M^{2+q/p}$ for a wedge of exterior angle $(p/q)\pi$.

3. Future plans

First, we will continue the LES of the trailing edge flow, and at the same time improve the numerical scheme to achieve higher computational efficiency. Grid-refinement studies will be carried out. Once a reliable, statistically convergent near-field solution is established, the velocity and wall-pressure statistics will be calculated and compared with the experimental measurements of Blake (1975). Cross-correlation and spectral analyses will be conducted to investigate the wall-pressure generation and scattering mechanisms.

The radiated far-field noise will be calculated following the framework outlined in Section 2.2. A remaining formulation issue to be addressed in the course of investigation is the treatment of the infinite, homogeneous spanwise direction in the source integral.

Acknowledgment

This work was supported by ONR grant N00014-95-1-0221.

REFERENCES

BLAKE, W. K. 1975 *A Statistical Description of Pressure and Velocity Fields at the Trailing Edge of a Flat Strut*, DTNSRDC Report 4241, David Taylor Naval Ship R & D Center, Bethesda, Maryland.

BLAKE, W. K. 1986 *Mechanics of Flow-Induced Sound and Vibration*, Vol. I and II, Academic Press, London.

BLAKE, W. K. & GERSHFELD, J. L. 1988 The aeroacoustics of trailing edges. In *Frontiers in Experimental Fluid Mechanics,* Chap. 10, (Gad-el-Hak, M. Eds.), Springer-Verlag.

BROOKS, T. F. & HODGSON, T. H. 1981 Trailing edge noise prediction from measured surface pressures. *J. Sound & Vib.* **78,** 69-117.

CHOI, H. 1993 Toward large eddy simulation of turbulent flow over an airfoil. *Annual Research Briefs-1993,* Center for Turbulence Research, Stanford University/NASA Ames, 145-149.

CRIGHTON, D. G. & LEPPINGTON, F. G. 1971 On the scattering of aerodynamic noise. *J. Fluid Mech.* **46,** 577-597.

CURLE, N. 1955 The influence of solid boundaries upon aerodynamic sound. *Proc. Royal Soc. Lond.* A. **231,** 505-514.

DURBIN, P. A. 1995 Separated flow computations with the k-ϵ-v^2 model. *AIAA J.* **44,** 659-664.

FFOWCS WILLIAMS, J. E. & HALL, L. H. 1970 Aerodynamic sound generation by turbulent flow in the vicinity of a scattering half plane. *J. Fluid Mech.* **40,** 657-670.

GERMANO, M., PIOMELLI, U., MOIN, P. & CABOT, W. H. 1991 A dynamic subgrid-scale eddy viscosity model. *Phys. Fluids A.* **3,** 1760-1765.

GOLDSTEIN, M. E. 1976 *Aeroacoustics*, Chap. 4, McGraw-Hill.

HOWE, M. S. 1978 A review of the theory of trailing edge noise. *J. Sound & Vib.* **61,** 437-465.

JANSEN K. 1995 Preliminary large-eddy simulations of flow around a NACA 4412 airfoil using unstructured grids. *Annual Research Briefs-1995,* Center for Turbulence Research, Stanford Univ./NASA Ames, 61-72.

KALTENBACH, H.-J. & CHOI H. 1995 Large-eddy simulation of flow around an airfoil on a structured mesh. *Annual Research Briefs-1995,* Center for Turbulence Research, Stanford Univ./NASA Ames, 51-60.

LIGHTHILL, M. J. 1952 On sound generated aerodynamically; I. General theory. *Proc. R. Soc. Lond.* A. **211,** 564-587.

LILLY, D. K. 1992 A proposed modification of the Germano subgrid scale closure method. *Phys. Fluids A.* **3,** 2746-2757.

LUND T. S. 1994 Large-eddy simulation of a boundary layer with concave streamwise curvature. *Annual Research Briefs-1994,* Center for Turbulence Research, Stanford Univ./NASA Ames, 185-195.

MITTAL R. 1996 Progress in LES of flow past a circular cylinder. Article in this volume.

NA, Y. & MOIN, P. 1996 Direct Numerical Simulation of Turbulent Boundary Layers With Adverse Pressure Gradient and Separation. *Report No. TF-68, Dept. of Mech. Engr., Stanford Univ.*

PAULEY, L. L., MOIN, P. & REYNOLDS, W. C. 1988 *Numerical Study of Unsteady Laminar Boundary Layer Separation*, Report No. TF-34, Dept. of Mech. Engr., Stanford Univ.

WANG, M. 1995 Aerodynamic sound of flow past an airfoil . *Annual Research Briefs-1995,* Center for Turbulence Research, Stanford Univ./NASA Ames, 257-271.

WANG, M., LELE, S. K. & MOIN, P 1996 Computation of quadrupole noise using acoustic analogy. *AIAA J.* **34,** 2247-2254.

ZAWADZKI, I., GERSHFELD, J. L., NA, Y. & WANG M. 1996 Hydroacoustic forcing function modeling using DNS database. *Proc. 1996 Summer Program,* Center for Turbulence Research, Stanford Univ./NASA Ames, 369-382.